scientific reports

Check for updates

OPEN

Theoretical modeling of hepatitis C acute infection in liver-humanized mice support pre-clinical assessment of candidate viruses for controlled-human-infection studies

Zhenzhen Shi[1,10], Adquate Mhlanga[1,10], Yuji Ishida[2,10], Ari Josephson[1], Nicholson T. Collier[3,4], Hiromi Abe-Chayama[5], Chise Tateno-Mukaidani[2], Scott J. Cotler[1], Jonathan Ozik[3,4], Marian Major[6], Jordan J. Feld[7], Kazuaki Chayama[8,9]✉ & Harel Dahari[1]✉

Designing and carrying out a controlled human infection (CHI) model for hepatitis C virus (HCV) is critical for vaccine development. However, key considerations for a CHI model protocol include understanding of the earliest viral-host kinetic events during the acute phase and susceptibility of the viral isolate under consideration for use in the CHI model to antiviral treatment before any infections in human volunteers can take place. Humanized mouse models lack adaptive immune responses but provide a unique opportunity to obtain quantitative understanding of early HCV kinetics and develop mathematical models to further understand viral and innate immune response dynamics during acute HCV infection. We show that the models reproduce the measured HCV kinetics in humanized mice, which are consistent with early acute HCV-host dynamics in immunocompetent chimpanzees. Our findings suggest that humanized mice are well-suited to support development of a CHI model. In-silico and in-vivo modeling estimates provide a starting point to characterize candidate viruses for testing in CHI model studies.

Keywords Hepatitis C virus, Agent-based modeling, Ordinary differential equations, Liver-humanized mouse model, Controlled human infection model

Approximately 57 million people were estimated in 2020 to have chronic hepatitis C virus (HCV) infection, with ~1.5 million new infections and ~300,000 HCV-related deaths per year[1]. The availability of highly effective direct-acting antivirals (DAAs) can cure more than 95% of infected individuals, however access to diagnosis and treatment is low worldwide and there is no vaccine to prevent new HCV infections, about 80% of which will become chronic[2,3], or re-infection in those who were cured by DAAs[4]. To accelerate the development of HCV vaccines, which is challenging[5], clinical trials for a controlled human infection (CHI) model have been recently suggested[6]. The design of a CHI model requires careful consideration of the key elements including viral clearance rates, timing of blood sampling intervals for immunological evaluations, and susceptibility of the virus to DAAs. These elements must be fully understood for development of a final study protocol[7]. Analyzing early viral-host kinetics immediately after infection and developing theoretical modeling tools are important

[1]The Program for Experimental and Theoretical Modeling, Division of Hepatology, Department of Medicine, Stritch School of Medicine, Loyola University Chicago, 2160 S. First Ave., Maywood, IL 60153, USA. [2]PhoenixBio Co., Ltd., Higashi-Hiroshima, Japan. [3]Decision and Infrastructure Sciences Division, Argonne National Laboratory, Lemont, IL, USA. [4]Consortium for Advanced Science and Engineering, University of Chicago, Chicago, IL, USA. [5]Center for Medical Specialist Graduate Education and Research, Hiroshima University, Hiroshima, Japan. [6]Division of Viral Products, Center for Biologics Evaluation and Research, Food and Drug Administration, Silver Spring, MD, USA. [7]Toronto Centre for Liver Disease, Toronto General Hospital, University Health Network, Toronto, ON, Canada. [8]Hiroshima Institute of Life Sciences, 7-21, Nishi Asahi-Machi, Minami-ku, Hiroshima-shi, Hiroshima 734-0002, Japan. [9]RIKEN Center for Integrative Medical Sciences, Yokohama, Japan. [10]These authors contributed equally: Zhenzhen Shi (theoretical [agent-based modeling] work), Adquate Mhlanga (theoretical [differential-equation modeling] work) and Yuji Ishida (experimental [in-vivo] work) . ✉email: chayama@mba.ocn.ne.jp; hdahari@luc.edu

aspects for addressing the aforementioned key elements to successfully develop the CHI model for testing HCV vaccine candidates.

Studying early acute HCV kinetics in people is notoriously difficult because infections are usually asymptomatic[8], although they may be recognized after iatrogenic exposures such as needle stick injuries, medical injection, needle sharing or other community exposures[8]. Our current understanding of early acute HCV-host dynamics is largely founded on data derived from infected chimpanzees using ordinary differential equations (ODEs)[9]. However, since June 2013, chimpanzees have no longer been available for biomedical research[10] and appropriate immunocompetent animal models for preclinical vaccine testing are lacking. Nevertheless, a two-step clinical trial in CHI was recently proposed. The first step is to define the challenge virus and to establish the viral-host kinetic picture in the absence of vaccination[7]. Existing chimeric mice with humanized livers that lack an adaptive immune response have the potential to serve as a preclinical model for studying early HCV-host interactions[11–13] for any candidate virus stock. In addition, the susceptibility of any inoculum to DAAs will need to be proven prior to administration to human volunteers[14]. Unless the donor of the challenge virus has a history of successful DAA treatment, this can only be performed in the humanized mouse model. However, detailed analysis of early virus kinetics in humanized mice from inoculation to steady state is lacking, since previous studies were performed during anti-HCV treatment after viral steady state was achieved[11–13].

Recently, we analyzed and modeled, using agent-based modeling (ABM), early hepatitis B virus kinetics from inoculation to steady state in chimeric urokinase type plasminogen activator (uPA)/severe combined immunodeficiency (SCID) mice reconstituted with humanized livers in the absence of the adaptive immune response[15,16]. The aim of the current study was to examine the early HCV kinetics in uPA-SCID-chimeric mice and to use both ODE and ABM approaches to explain the observed kinetic patterns. The secondary aim was to compare the ODE and ABM approaches to provide insights into the utility of the two modeling tools for simulating early virus-host dynamics that could be used in the CHI model.

Materials and methods

Experiment setup

Five uPA+/-/SCID chimeric mice with humanized livers (PXB SCID-MhL, with hepatocyte donor: JFC [1 year, male Caucasian, purchased from In Vitro Technologies, Baltimore, MD, USA]) were produced as described previously[17]. Briefly, 1-2.5 × 10^5 cells were transplanted into 2–4 week old uPA$^{+/-}$/SCID mice via intrasplenic injection. Replacement index of human hepatocytes in each mouse was estimated by blood human albumin levels measured by latex agglutination immunonephelometry (LX reagent "Eiken" Alb II; Eiken Chemical Co., Ltd., Tokyo, Japan) as described[17]. Ten male mice (5 PXB SCID-MhL, human albumin > 9 mg/mL (estimated replacement index > 80%)), and 5 SCID mice without humanized livers (SCID-M) were inoculated intravenously with HCV positive serum (genotype 1a, AB520610) at 1 × 10^6 RNA copies/animal. Serum HCV RNA titers were measured at 1 min, 30 min, 1 h and 6 hr, and days 1, 2, 3, 4, 6, 8, 10, 12, 14, 21, 28, and 35 post infection (p.i.) using quantitative real-time PCR as previously reported[18]. Mice were anesthetized with isoflurane using the MK-AT210 anesthesia machine for small animals as recently suggested[19]. A concentration of 4% was used for induction, 1.5% for blood collection, and 2% for sacrifice, followed by cervical dislocation. All methods were performed in accordance with the relevant guidelines and regulations of Hiroshima University. The experimental protocol was approved by the Ethics Review Committee for Animal Experimentation of the Graduate School of Biomedical Sciences, Hiroshima University (A14-195) in accordance with the ARRIVE guideline.

Ordinary differential equation model for HCV dynamics

We modified our previous model for acute HCV dynamics in chimpanzees[9] by excluding adaptive immune response features of immune-related death of infected cells and noncytolytic clearance. The development of the proposed ODE model (Fig. 1) is described in detail in the Supplementary Material. The mathematical model is described by the following ODE model equations.

$$\begin{aligned}
\frac{dT}{dt} &= -dT - \beta_e V_e T - \beta_m V_m T\left(1-\eta\left(t\right)\right)\\
\frac{dI}{dt} &= \beta_e V_e T + \beta_m V_m T\left(1-\eta\left(t\right)\right) - \delta_0 I\\
\frac{dV_e}{dt} &= -cV_e\\
\frac{dV_m}{dt} &= pI\left(1-\epsilon\left(t\right)\right) - cV_m
\end{aligned} \tag{1}$$

T represents the number of uninfected human hepatocytes (i.e., target cells), I is the number of infected human hepatocytes, V_e is the inoculated viral load, and V_m represents the productive viral load produced by human hepatocytes. The model assumes that target cells have a death rate of d and are susceptible to *de novo* infection with rate constants β_e and β_m for the inoculated and productive viruses, respectively. Infected cell death/loss rate is represented by δ_0. A time-dependent blocking of infection and blocking of production is represented by the step functions $\eta\left(t\right)$ and $\epsilon\left(t\right)$, respectively. The time when the step functions change from zero to η or ϵ is denoted by t_{ir}. After this time, either blocking of production or blocking of infection occurs, both most likely representing innate immune response mechanisms. These terms capture how innate immunity limits viral spread, either by reducing viral production or preventing new infections in humanized mice lacking adaptive immune responses. Virions (V_m) are produced with rate p, and are cleared with a rate constant c. We assume that V_m and V_e are cleared with the same rate.

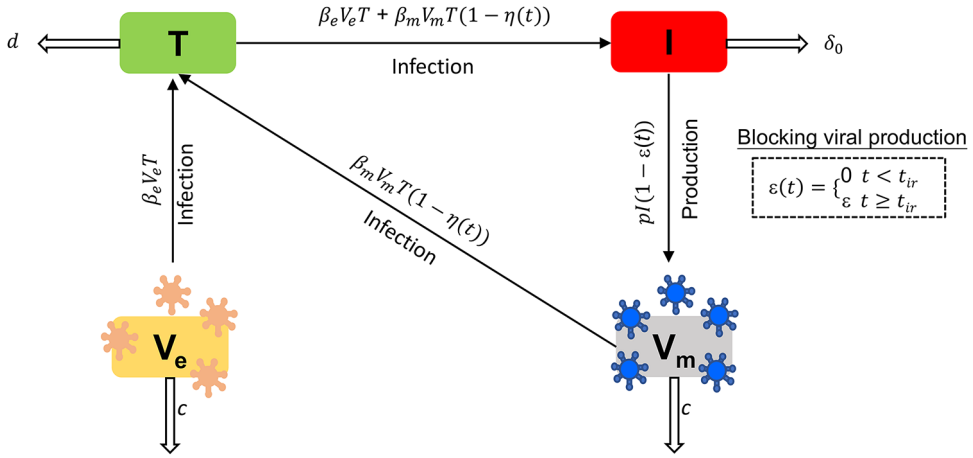

Fig. 1. Schematic diagram of the ODE model (Eq. 1, two-viral population model). V_e denotes the inoculated virus population and c is the viral clearance rate constant from blood. V_e infects human hepatocytes (termed cells), T, at a rate β_e. Uninfected cells die at a rate d. I represents HCV-infected cells, which produce virions at a production rate p, that die at a rate δ_0. The virus V_m, produced by HCV-infected cells (I), infects uninfected cells at a rate β_m. ε(t) and η(t) represent the possible time dependent efficacies in blocking viral production ($0 \leq \varepsilon \leq 1$) and infection ($0 \leq \eta \leq 1$), respectively, that begins at t_{ir} post infection. Uninfected and infected human hepatocyte death were set to 0 (i.e., $d = \delta_0 = 0$).

Initial model parameter values

We used an initial human hepatocyte count of $T_0 = 3.0 \times 10^8$/mL that was previously estimated based on the approximate human albumin (hAlb) level of each mouse and weight in a recent study for uPA-SCID-chimeric mice[20]. We assumed that the initial count of infected human hepatocytes is $I_0 = 0$ and therefore initial $V_{m0} = 0$. Since there is no evidence of human hepatocyte death or significant proliferation during infection as can be reflected, in part, by stable hAlb levels[21], we set $d = \delta_0 = 0$. The inoculated virus V_{e0} for mouse 1, 2, 3, 4, and 5 was set to measured data at 1 min after inoculation, 1.62×10^6, 1.52×10^6, 0.97×10^6, 0.99×10^6, and 1.31×10^6 copies/mL, respectively. We assume that blocking of infection ($\eta = 0$) and blocking of production ($\epsilon = 0$) until time t_{ir} post-inoculation.

Parameter estimation for the ODE model

The inoculated virus (V_e) clearance rate c was computed using a linear regression model with time samples at 1 min, 30 min, 1 h and 6 h from the scikit-learn Python library (Version 0.24.1). We assumed that the sample at 6 h was below 6000 copies/mL, corresponding to the limit of detection for the quantitative real-time PCR, and was set to 6000. Therefore, the computed c is considered as a minimal estimate for c. The infection rate of the inoculated virus could not be estimated with confidence, and therefore it was fixed at $\beta_e = 1 \times 10^{-11}$ mL/virions/day (or 4.17×10^{-13} mL/virions/hour) as described in Supplementary Material C.

We applied the following two steps to estimate the remaining unknown parameters by fitting the ODE model to the HCV kinetics for each mouse. A first pass for fitting β_m, ε, and p was done using the curve fit feature Berkeley Madonna (Version 8.3.18) with the default values of all the above estimated parameters (initial model parameters and parameter c), with $V_{tot} = V_e + V_m$ used to fit to the data. The best fit values obtained from Berkeley Madonna were used as initial guesses in a Python Jupyter Notebook (Version 6.3.0). It is important to note that during the Python analysis, we kept β_e, t_{ir} fixed in order to avoid identifiability issues. The remaining parameters β_m, ε, and p were fitted with the lmfit library (Version 1.1.0) using the least squares method. The lmfit Python library was utilized to determine the 95% confidence intervals for the final three fitted parameters (β_m, p, ε).

Agent-based model (ABM) for HCV dynamics

We modified our recently developed ABM[15] for acute hepatitis B virus infection in humanized mice to study acute HCV kinetics in these mice. To summarize, we created two types of agents to account for human hepatocytes and virus (V). Depending on the time of interacting with virus, individual human hepatocyte cells can be in one of the following three discrete states: uninfected susceptible target (T), infected cell in eclipse phase (I_E) (i.e., not yet releasing progeny virus), or productively infected cell secreting progeny virus (I_p) (Fig. 2). An eclipse phase parameter was assigned to individual in-silico human hepatocyte to account for the time duration before virus secretion begins after infection as previously reported in vitro[22]. The ABM execution is an iterative process where each iteration represents a discrete time step, where 1 step = 1 h. For each iteration, a portion of uninfected susceptible hepatocytes (T) are infected and then proceed to an eclipse phase (I_E). After the eclipse

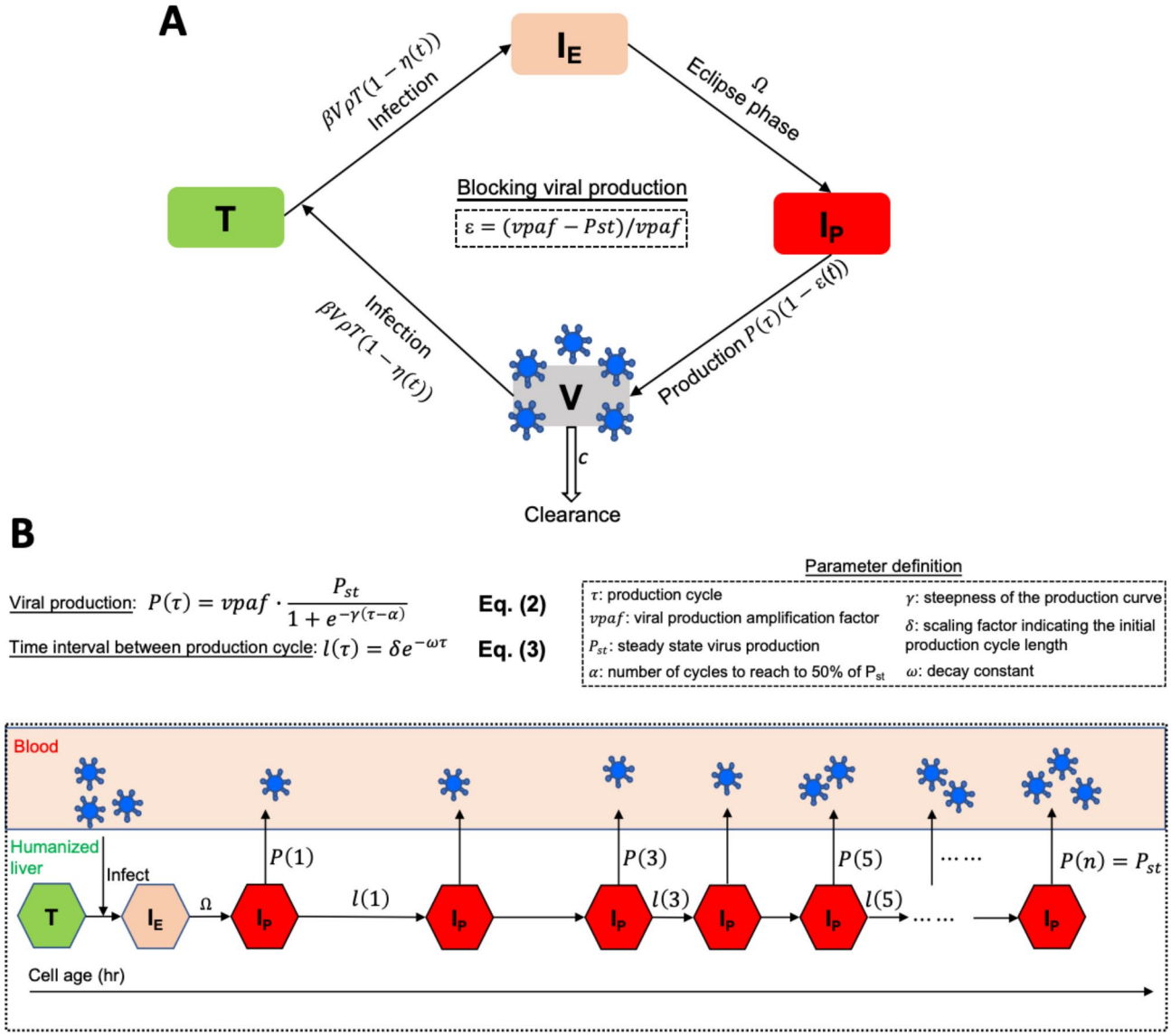

Fig. 2. Schematic diagrams of the ABM model. (**A**) The human hepatocytes can be only in one of the following three phases at a given time: (i) T, uninfected cells which are termed as target or susceptible cells, (ii) I_E, HCV-infected cells in eclipse phase (i.e., not yet releasing virions), and (iii) I_p = productively HCV-infected cells (i.e., actively releasing virions). The free virus in blood, V, is composed of infectious and non-infections virions. The parameter ρ represents the fraction of virions that are infectious, β represents the infection rate constant, Ω represents eclipse phase duration, c, represents viral clearance from blood, and $P(\tau)$ (Eq. 2) represents virion secretion from I_P. Blockage of viral production and viral infection, starting at time t_{ir} post infection, are modeled with efficacy $\varepsilon(t_{ir})$ and $\eta(t_{ir})$, respectively. We assume (as in the ODE model, Fig. 1) that uninfected and infected human hepatocytes do not die during the 35 days of experiment. (**B**) Schematic diagram of viral production cycle for an individual human hepatocyte. $P(\tau)$ is the number of virions produced by an infected cell, and $l(\tau)$ is the time interval between production cycle (time unit: h). The virions were initially released by I_p starting with a high production rate of $P(1)$ virion per cell with a long production cycle of $l(1)$ that gradually reaches a production of $P(3)$ virions per cell with a shorten production cycle of $l(3)$ and then proceeds to $P(5)$ virions per cell per $l(5)$ before virion production increases to reach to a steady state production rate of P_{st} virions per hour per cell.

phase, I_E become productive (i.e., I_p) and start to release a new generation of progeny virus particles through its production cycle (Eq. 2 and Eq. 3).

$$P(\tau) = \begin{cases} vpaf \bullet \frac{P_{st}}{1+e^{-\gamma(\tau-\alpha)}} & t \le t_{ir} \\ \frac{P_{st}}{1+e^{-\gamma(\tau-\alpha)}} & t > t_{ir} \end{cases} \quad (2)$$

where $P(\tau)$ is number of virions produced by infected cells at a production cycle of τ. P_{st} is steady state virus production, α is number of cycles to reach to 50% of P_{st}, γ is the steepness of the production curve, and t_{ir} is the time when innate immunity starts to take effect (Table 2). To account for the biphasic HCV increase with (or without) a transient decline observed in HCV RNA kinetic data (Fig. 3), we multiplied $P(\tau)$ with a constant parameter *vpaf*, representing a high production rate before t_{ir}, to simulate assumed blockage of viral production, i.e., parameter ε in Fig. 2A, or blockage of viral infection i.e., parameter η in Fig. 2A, reminiscent of our previous observation of such biphasic viral increase with (or without) a transient HCV decline seen in chimpanzees[9].

$$l_\tau = \delta e^{-\omega\tau} \quad (3)$$

where l_τ is interval between production cycles, τ is the production cycle, δ is scaling factor indicating the initial production cycle length, and ω is decay constant. A schematic picture of the modified ABM is shown in Fig. 2.

ABM parameter estimation

The initial uninfected human hepatocyte number (T_0), initial viral loads (V_{e0}) and HCV clearance rate constant from blood (c) were set as described above and in Table 1. The fraction of infectious HCV in blood is not known, therefore was arbitrary set as ρ = 0.5. Using predefined parameter ranges based on preliminary fits using AnyLogic, we applied a genetic algorithm (GA) to fit the ABM with the mice experimental data (Table 2). The objective of the GA was to find the parameter combination which can achieve the least j-score of mean of ten replicates with different random seeds. The GA was implemented using the DEAP[23] evolutionary computation Python framework (specifically[24]: Chap. 7) and integrated into an EMEWS high-performance computing workflow using EMEWS queues for Python[25]. The use of high-performance computing resources enables the concurrent evaluation of large numbers of design points, reducing the time to solution. During each iteration of the GA, the best points from the currently evaluated population are selected using a tournament selection method to create a new population. Each of these points was then mated with another according to a crossover

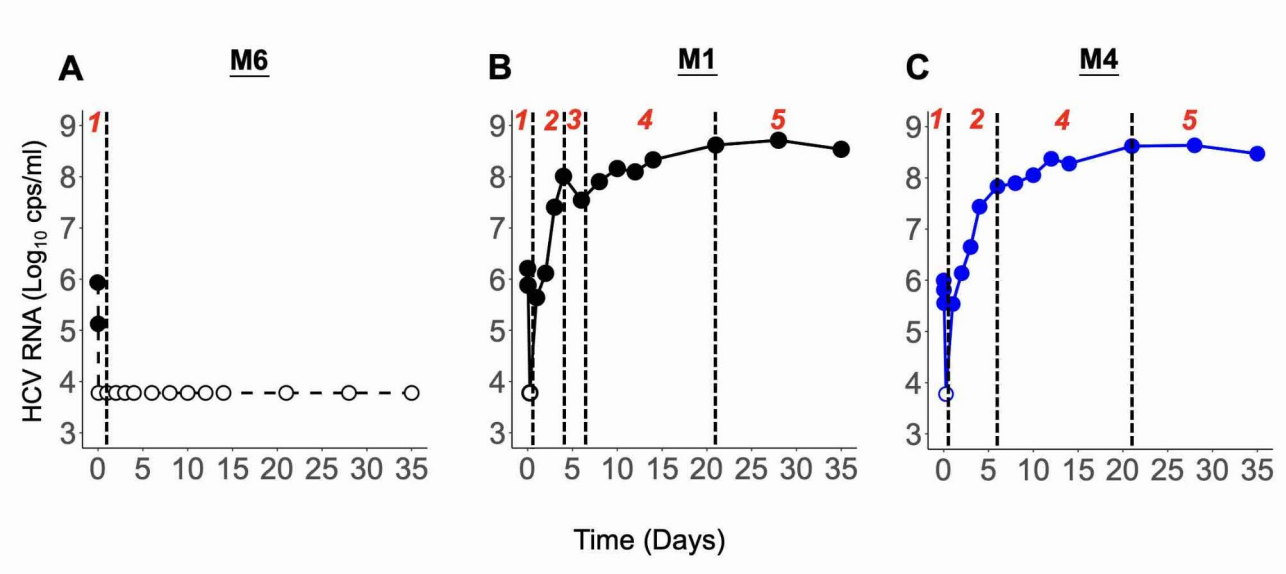

Fig. 3. Kinetics of acute HCV infection in SCID mice. (**A**) Representative HCV kinetics in SCID-M mice, consistent with the absence of human hepatocytes (M6). Only Phase 1 was observed in all five SCID-M mice. (**B**) Representative HCV kinetics in 3 (out of 5 shown in Fig. 4) SCID-MhL mice, consistent with human hepatocytes (M1): Phase 1, rapid viral decline; Phase 2, rapid viral increase; Phase 3, transient decline; Phase 4, slower viral increase; Phase 5, steady state. A transient decline was observed between the two increase phases (Phases 2 and 4) around day 5. (**C**) Representative HCV kinetics in 2 (out of 5 in Fig. 4) SCID-MhL mice (M4) with 4 phases observed (without Phase 3: transient decline as shown in (**B**): Phase 1, rapid viral decline; Phase 2, rapid viral increase; Phase 4, slower viral increase; Phase 5, steady state. Solid black circles represent measured HCV RNA level and empty circles represent HCV RNA level lower than quantifiable limit (< 6000 copies/mL).

Parameter	Symbol [unit]	ODE estimates					
		M1	M2	M3	M4	M5	Median [Min, Max]
Virion clearance rate	$c^{\star}$ [1/hr]	0.93	0.87	0.86	0.85	0.90	0.87 [0.85, 0.93]
Infection rate of virions produced by the mouse	β_m (10^{-11}) [mL/virions/hr]	3.2 [0.8–6.5]	5.1 [1.86–13.1]	6.5 [2.3–17.8]	10.7 [5.2–22.5]	2.3 [0.8-5.0]	5.1 [2.3, 10.7]
Virion production rate before t_{ir}	p [virions/cell/hr]	15.4[#]	11.2 [4.7–28.9]	8.1 [3.1–21.5]	8.3 [4.0-16.7]	27.1 [10.3–81.3]	11.2 [8.1, 27.1]
Time at virion production drops	t_{ir}[†] [day]	3.5	3.0	2.8	1.7	2.8	2.8 [1.7, 3.5]
Efficacy in blocking viral production	ε	0.92 [0.88–0.96]	0.92 [0.87–0.95]	0.91 [0.85–0.94]	0.91 [0.85–0.94]	0.95 [0.92–0.97]	0.92 [0.91, 0.95]
Virion production rate after t_{ir}	p (1-ε) [virions/cell/hr]	1.23	0.90	0.73	0.75	1.36	0.90 [0.73, 1.36]

Table 1. Results of the ODE model fit parameters. Parameter $c^{\star}$ was estimated using linear regression via scikit-learn's least squares method (Version 1.3.0). A first pass for fitting β_m, ε, p and t_{ir}[†] was done using the curve fit feature Berkeley Madonna (Version 8.3.18) using the values for the other parameters given in Sect. 2.2.1. Parameters β_m, p, and ε were fit in Python with 95% confidence intervals in brackets. [#]Value for p for M1 was estimated without confidence. The upper bound for the confidence interval was infinity. t_{ir}[†] could not be fit with confidence, hence we had to base our estimates with Berkeley Madonna. $\beta_e = 1 \times 10^{-11}$ mL/virions/day (4.17×10^{-13} mL/virions/hour).

Category	ABM parameters			GA best estimates[#] [min – max][**]				
	Description	Symbol [unit]	Initial range[*]	M1	M2	M3	M4	M5
Infection	Infection rate	β (10^{-11}) [cell/hr]	[3.3–66.7]	15.7 [NA]	18.5 [13.7–18.5]	22.2 [NA]	20.6 [NA]	13.7 [13.3–14.7]
Eclipse phase	Min eclipse phase	Ω_{min} [hr]	[1–20]	2 [NA]	1 [1–3]	2 [NA]	2 [NA]	2 [NA]
	Max eclipse phase	Ω_{max} [hr]	[1–60]	39 [39–40]	38 [38–55]	51 [50–52]	38 [38–48]	52 [NA]
Viral Production (Eq. 2, and 3; Fig. S3)	Initial production cycle length	δ [hr]	[1–20]	8.5 [8.5–10.3]	10.9 [8.5–14.8]	10.9 [10.7–10.9]	9.6 [9.6–10.9]	12.0 [12.0-12.9]
	Decay constant	ω [hr^{-1}]	[0.1-2]	0.9 [0.9–1.4]	1.9 [0.9–1.9]	1.2 [1.2–1.4]	1.3 [1.3–1.9]	0.4 [0.4–0.5]
	Number of cycles to reach 50% of P_{st}	α [hr]	[1–60]	52.1 [39.7–54.3]	33.9 [32.5–41.0]	33.1 [1.0-33.1]	6.6 [5.5–57.8]	21.5 [20.5–40.5]
	Steepness of the production curve	γ [hr^{-1}]	[0.1-2]	1.6 [0.8–1.6]	1.1 [0.7–1.7]	0.4 [0.3–0.6]	0.4 [0.2–0.5]	1.5 [0.1–1.6]
Blocking viral Production (Fig. S3)	Viral production amplification factor	*vpaf* [virion/hr]	[1-240]	30 [29–30]	18 [18–26]	14 [NA]	16 [16–20]	150 [139–150]
	Time at virion production drops	t_{ir} [day]	[72–168]	4.1 [NA]	4.1 [4.0-4.8]	4.9 [4.8-5.0]	4.9 [NA]	4.1 [4.0-4.2]
	Virus production at steady state after t_{ir}	P_{st} [virion/cell/hr]	[1–5]	1 [NA]	1 [NA]	1 [NA]	1 [NA]	1 [NA]
	Efficacy in blocking viral production	ε [%]	[0–1]	96.7 [96.6–96.7]	94.3 [94.3–96.2]	92.6 [NA]	93.7 [93.7–95.0]	99.3 [99.29–99.33]

Table 2. Best estimated ABM parameters using genetic algorithm (GA). *: The initial parameter ranges were obtained based on preliminary ABM fits done using AnyLogic. The objective function of GA is to minimize the difference between experimental data and simulated results. J-score represents the mean squared error (MSE) of ten replicates with different random seeds for a parameter combination. [#]: Best model fits, i.e., with the least J-scores, are shown in Fig. 4. **: The parameters min and max ranges of the GA fits represent top 50 J-scores from a total number of 2524, 2503, 2500, 2619, and 2597 simulation fits for mice 1 (M1), 2 (M2), 3 (M3), 4 (M4), and 5 (M5), respectively. NA, not applicable since minimum = maximum. ε representing efficacy in blocking viral production was calculated using the formula: ε = (*vpaf* - P_{st})/*vpaf*.

probability and, finally, each of the resulting points was mutated according to a mutation probability. At each GA algorithm iteration, the new population is evaluated in parallel, and the evaluation results were gathered. The GA population size was set to 204, the mutation probability to 0.2, the crossover probability to 0.5, and the number of iterations to 20. The runtime for a typical run was 4.8 h using full concurrency on 6 nodes (with 36 cores per node), or about 1037 core hours.

Results

HCV RNA kinetics

In both SCID-M (absence of human hepatocytes) and SCID-MhL (humanized hepatocytes) mice, HCV rapidly declined from ~6 $\log_{10}$ RNA copies/mL to below the assay quantifiable limit (< 3.8 $\log_{10}$ RNA copies/mL) during the first 6 h following inoculation (Fig. 3). There was no difference in HCV decline rate during the first 6 h p.i. between SCID-M and SCID-MhL mice. A productive infection was established in SCID-MhL mice (Fig. 3B and C, Fig. 4), but not in SCID-M mice, following the initial 6 h time point. Overall, the infection followed a consistent pattern of 5 distinct phases. After the initial decline in viral load (Phase 1) within the first 6 h, there was a rapid increase in HCV until day 4–5 p.i. (Phase 2). This was followed by a slower increase in viral load (Phase 4). Mice 1, 2, and 5 exhibited a transient decline (Phase 3) between the two periods of increase (Phases 2 and 4), occurring around days 4 to 5. The viral load stabilized at an average of 8.51 ± 0.17 $\log_{10}$ RNA copies/mL 10 to 20 days p.i., for all 5 mice (Phase 5), which was maintained throughout the remainder of the study period.

ODE modeling results

The basic model with one virus population (Supplementary Material A, Fig. S1A) or with an eclipse phase (Supplementary Material B, Fig. S1B) could not fit the observed initial rapid viral decline (Fig. 3B and C, Phase 1). To explain the initial rapid decline, a model with two virus populations (Eq. 1) was developed. This model reproduced the initial rapid viral decline well (Fig. 4and Fig. S1C), assuming that the inoculated virus was less infectious (60 to 260-fold, Table 1) compared to newly produced virions from infected human hepatocytes.

After the initial rapid viral decline that reached undetectable RNA levels (Fig. 3B and C, Phase 1), the virus resurged in a biphasic manner, i.e., a rapid phase during the first 2 to 6 days p.i. followed by a slower phase. A transient decline was observed in 3 mice in between these phases, and the virus eventually stabilized at high steady state levels in all 5 mice (Figs. 3 and 4). Modeling suggested that a transient decline that resulted in biphasic viral increase (Fig. 3B), can be best explained by assuming blockage in viral production (Fig. S2, bottom row) rather than blocking of infection (Fig. S2, top row) (see Supplementary Material D for more details). Therefore, we assumed that blocking viral production by an innate immune response was the main mechanism to explain the biphasic viral increase across all mice, reminiscent of the observed biphasic increase in chimpanzees that was attributed to an endogenous type I interferon response[9]. While we cannot completely exclude the possibility that blocking of infection contributed to the transient viral decline (Phase 3), blocking of infection was fixed to zero in the model because it cannot be estimated simultaneously with blocking of viral production.

The ODE model provided HCV kinetic parameters that are detailed in Fig. 4, blue dashed lines and Table 1. Modeling indicated that the median half-life of HCV in the serum of mice was 48 [min-max: 45–49] minutes. Modeling estimated a median efficacy $\varepsilon = 92\%$ [min-max: 91–95%] in blocking viral production that occurred at time $t_{ir} = 2.8$ [1.7–3.5] days p.i. The median virion production rate was estimated as 11.2 [8.1–27.1] virions/cell/hr and 0.9 [0.7–1.4] virions/cell/hr before and after t_{ir}, respectively.

ABM results

The ABM reproduced the multiphasic HCV kinetic patterns observed in humanized mice (Fig. 4, blue solid lines). The estimated ABM parameters for all mice are shown in Table 2. Interestingly, the median infection rate $\beta = 18.5 \times 10^{-11}$ [min-max: 13.7×10^{-11} – 22.2×10^{-11}] cell/h is similar for all 5 mice. The ABM predicts a variable eclipse phase (Ω) ranging from 1 to 52 h with a median minimal value $\Omega_{min} = 2$ [1–2] h and a median maximal value $\Omega_{max} = 39$ [38–52] h (Fig. S3, shaded box), reminiscent of the ~2-day delay before JFH-1 virus increased post infection in Huh-7.5.1 cells[26].

The ABM predicts that after the eclipse phase, viral release from productively infected cells starts slowly with a long production cycle of 18 virions [14–150] per 11 h [9 − 12] that gradually decreases to 18 virions [14–150] per hour after ~1–2 days, resulting in increased viral production (Fig. S3). The eclipse phase durations did not affect the amount of virion production or the gradual decrease in the duration of the production cycle (Fig. S3, shaded box).

Two parameters were incorporated into the ABM (as in the ODE modeling approach) to account for blocking of viral production (ε) or infection (η), respectively, at time t_{ir} post infection to predict the observed biphasic viral expansion. Modeling results indicated that blocking of viral production provides a better goodness of fit (i.e., lower mean squared error as shown in Table S1) compared to solely blocking of infection (Fig. 4, and Fig. S2). While we cannot completely rule out an effect in slowing infection due to identifiability issues, to estimate simultaneously both ε and η, we set $\eta = 0$. Modeling results indicate a median efficacy $\varepsilon = 94.3\%$ [92.6–99.3%] in blocking viral production that started at a median $t_{ir} = 4.1$ [4.1–4.9] days p.i., after which the virion production cycle decreased to 1 virion/cell/h, where it remained until viral steady state was reached (Table 2).

Comparing the ODE and ABM approaches

A detailed comparison of the ODE and ABM approaches and predictions is summarized in Table S2. Differences in the two modeling approaches were particularly relevant regarding the eclipse phase and infected cell productivity. Based on an early study regarding replication of HCV in cell culture[22], an eclipse phase was detected before virion production. The ABM was better able to capture the specific dynamics and timing of the eclipse phase and to simulate the decreasing viral production cycle as HCV production increased in Phase 2. The dynamics and timing of the eclipse phase were not well represented in the ODE due to the assumption of homogeneity and averaging. Therefore, the ABM was used to predict the eclipse phase and subsequent virion production cycles (Table 2 and Fig. S3). The ODE model suggested that the inoculated virus and the virus produced by infected human hepatocytes represented two different viral populations, where the former was 100-fold less infectious than the latter (Table S2). A potential advantage of the ODE is that it did not require that infected cells produce an integer value of virions per average unit time. In addition, the ABM required

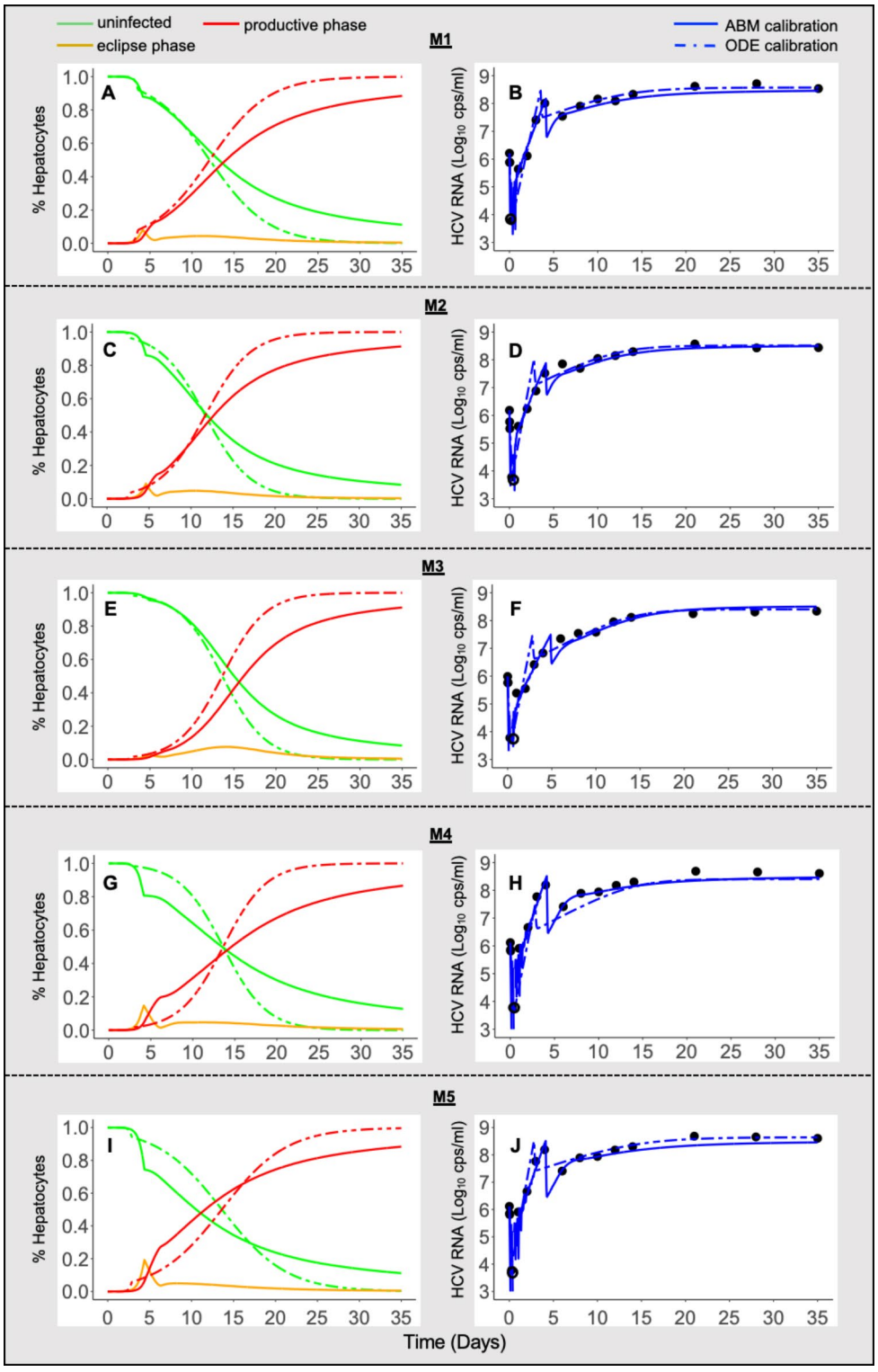

Fig. 4. Comparison of model calibration between ODE approach (dashed lines) and ABM approach (solid lines) in all five liver-humanized (SCID-MhL) mice. Serum HCV RNA kinetics were depicted using solid black circles. Green curves represent the percentage of uninfected cell (T), yellow curves represent the percentage of cells in eclipse phase (I_E), red curves represent the percentage of cells in the productive phase of infection (I_p), and blue curves represent the HCV RNA level (V). The optimal parameter combination was incorporated into the ODE (Table 1) and ABM (Table 2) models to obtain the HCV kinetic trajectory for each mouse by assuming blocking viral production (denoted as ε). HCV RNA levels lower than the quantifiable limit (< 6000 copies/mL) are shown using empty circles.

substantially greater computational cost than the ODE. The models yielded slightly different predictions such as a higher rate of infection of uninfected hepatocytes for the ODE and a higher efficacy of immune mediated blocking of viral production for the ABM. Both models indicated that immune mediated blocking of viral infection cannot explain the observed biphasic viral increase in all humanized mice (Fig. S2).

Comparison of analysis and modeling HCV kinetics in humanized mice and chimpanzees

Observed kinetics and model parameters for HCV replication in vivo were compared between the chimpanzee model[9] and the humanized liver mouse model (Table 3). While the majority of chimpanzees were infected with $\leq$1170 HCV RNA copies, the humanized mice were inoculated with a higher viral load ($\sim 1\times10^6$ RNA copies) and had more frequent data sampling during the first 6 hr p.i. allowing us to capture the rapid viral decline and estimate HCV $t_{1/2}$ of 48 min. An earlier (12–22 vs. 28–56 days) and higher viral plateau (8.5 vs. 6.1 log cp/mL) was reached in humanized mice compared to the chimpanzees.

Both in vivo models showed that the HCV increase p.i. was biphasic with a transient viral decline in between, in most cases. In silico modeling in both in vivo models predicted an efficacy in blocking viral production of about 90%, that started several days p.i. The chimpanzee and humanized mouse models were similar in terms of the observed HCV biphasic increase, the timing of the transient viral decline, and the predicted blocking of viral production and its efficacy in spite of the uncertainty regarding the number of susceptible cells (hepatocytes) in the chimpanzee model along with a $\sim$3 order of magnitude lower estimated infection rate in the chimpanzee model compared to the humanized mouse model.

Discussion

To add valuable layers of understanding to the complex interplay between HCV and the host, we applied ODE and ABM approaches to examine the early HCV kinetics from inoculation to steady state in uPA-SCID-chimeric mice with humanized livers. While there are differences in the modeling approaches, both models can explain the observed viral kinetics and provide important insights into the dynamics of acute HCV infection. Modeling indicated that the median HCV half-life ($t_{1/2}$) equals 48 min in humanized mice, consistent with the HCV $t_{1/2}$ estimated in patients undergoing liver transplantation[27]. After a rapid viral decline, during which newly infected hepatocytes were not producing progeny virus, multiphasic HCV kinetic patterns were observed in the humanized mice, which were consistent with our previously reported kinetics in chimpanzees after HCV inoculation and before seroconversion[9]. Moreover, the transient decline resulted in a biphasic viral increase seen in the humanized mice can be explained by a partial blockage of virion production possibly due to an early stage innate immune response in the human liver cells, consistent with the observed biphasic increase in chimpanzees that was shown to correlate with the induction of intrahepatic 2OAS-1 mRNA expression, a type I interferon-induced gene[28].

The ODE model was adapted from a prior chimpanzee model[9]. Qualitatively, both the humanized mouse and chimpanzee models exhibit similar features, although the speed of the kinetics differs. As seen in chimpanzees before seroconversion, the virus in the mice had a biphasic increase with a transient decline in between, before HCV levels reached a steady state consistent with chronic infection. Compared to the chimpanzees, the mice had a transient decline 3–12 days earlier and reached steady state 26–34 days earlier (Fig. 4[9]). Additionally, both the mice and chimpanzee models suggest that the biphasic increase is due to blocking of HCV production, with a similar efficacy of 90–95% in mice and 85–95% in chimpanzees, rather than a blocking of infection. The mechanism for blocking of virion production in chimpanzees was suggested to be through an endogenous type

Parameter description [units]	Chimpanzees	Humanized Mice (Table 1)	Source
Inoculation quantity [copies]	$\leq$ 1170 HCV RNA copies as described in [19]*	1×10^6	Experimental design
Viral clearance from circulation (range), c [1/day]	Fixed** to 6.0	20.6–22.2	Math modeling
Time (range) p.i. of blocking of viral production, t_{ir} [days]	5.3–15.5	1.7–3.5	Math modeling
Efficacy (range) of blocking of viral production, ε [%]	85–95	91–95	Math modeling
Viral production (range), p [virions/cell/day]	0.1–317	188–585	Math modeling
Infection rate (range), $\beta_{(m)}$ [mL/virions/day]	$0.1–11\times10^{-7}$	$0.8–22.5\times10^{-11}$	Math modeling
Number of susceptible hepatocytes, T_0 [cells/mL]	Fixed[&] to 1.87×10^6, 1.87×10^7 or 1.87×10^8	Fixed to 3×10^8	Math modeling
Mean ± SD plateau HCV RNA concentration [Log copies/mL]	6.1 ± 0.5	8.5 ± 0.17	Experimental observation
Time (range) to reach plateau [days]	28–56	12–22	Experimental observation

Table 3. Comparison of parameter values obtained from chimpanzee[9] and mice ODE models. *, Briefly, 7 chimpanzees were infected by acute-phase plasma from another chimpanzee with 1170 ($n=6$) and 39 ($n=1$) HCV RNA copies. Three chimpanzees were infected with an estimated range of 0.01–40 H77-RNA (genotype 1a) copies into the liver. Two chimpanzees received more than 1170 RNA copies, one received 3000 µg and a second received 22 µg of in vitro transcribed RNA. **, Could not be estimated therefore was fixed based on previous literature. [&], Due to the uncertain number of susceptible hepatocytes in the liver a range of initial hepatocyte count was used. SD, Standard deviation.

I interferon response[9] and was confirmed through analysis of intrahepatic cytokines[28]. The humanized mouse model provides a means to further explore the nature of blocking HCV production in human hepatocytes, as hepatocytes can mount an innate immune response and produce type 1 interferons but lack an adaptive response. Lastly, we found that the HCV steady state level was about 100-fold higher, at an average of 8.5 $\log_{10}$ copies/mL in mice compared to 6.1 $\log_{10}$ copies/mL in chimpanzees. Higher levels of HCV at steady state (chronic infection) could reflect the lack of an adaptive immune response in the mouse model. In chimpanzees, HCV titers decreased exponentially following ALT elevations and seroconversion to HCV-specific antibodies[9], which coincide with T cell infiltration in the liver and increases in intrahepatic cytokine levels[28,29], indicating that the adaptive immune response impacts viral replication in chronic infection. The decrease in HCV RNA titers coincident with ALT elevations in chimpanzees has also been observed in human infections[8]. Overall, the similarity between the two models suggests this mouse model is well-suited to simulate early acute HCV infection.

As the only readily available animal model of acute HCV infection, the liver-humanized mouse model will almost certainly play a critical role in the safe development of a CHI model. Any proposed candidate viruses will have to exhibit standard and reproducible acute phase kinetics and must be shown to be susceptible to DAAs. It is straightforward to acquire an HCV sample from an infected person before successful DAA treatment. However, obtaining acute phase kinetics from patients is impractical since recognition of acute HCV is uncommon except in immunosuppressed solid organ transplant recipients from HCV-infected donors[30]. In addition, it has been acknowledged that using virus isolated from a chronically infected individual will introduce further complications, such as the presence of immune complexes that markedly reduce the viral infectivity levels and thus require a larger inoculum to be used[14]. An alternative approach would consist of inoculating a human volunteer with RNA transcribed in vitro from an infectious clone[14]. Samples would then be collected from the volunteer to provide the final inoculum for subsequent studies in the CHI model. However, prior to this, studies would have to be performed in the humanized mouse model to verify the infectiousness of the in vitro transcribed RNA and the susceptibility of the virus to DAAs. Indeed, a previous mathematical modeling study in humanized mice during anti-HCV treatment evaluated treatment efficacy and predicted drug mode of action[11]. Our modeling data provide support for the use of the humanized mouse model to assess the characteristics of candidate challenge viruses, regardless of the source.

As recently proposed[7], the first step in developing a CHI model is to characterize the kinetics of viral replication and the immune response in the absence of vaccination. A dose of > 1000 HCV RNA copies, similar to that used in chimpanzee infections, is anticipated to establish consistent HCV infection and subsequent immune responses in humans[14]. Our modeling data from the humanized mice indicate that there could be an effect of infectious dose on viral kinetics (Fig. S4). Both models predict a time delay in reaching steady state of early viral kinetics in the mouse model with low titer inoculum. Previous studies have shown that infectious dose does not impact the outcome or acute phase viral titers in chimpanzees[28,31]. However, the blood volume to viral particle ratio would be much lower in the mouse model than the chimpanzee model, which may influence the impact of lower titers in the mouse system as previously reported during acute HBV infection[15,16]. To define the infectious dose, a small-scale inoculation study in a few participants of the CHI model has been suggested[14,32]. In such a study one volunteer would be infected at a low dose, and after infection is demonstrated, a small number of additional volunteers (3–4) would be infected[14,32]. Using the collected viral kinetics in the inoculation study in volunteers, modeling approaches developed in the current study could be used to test the reproducibility of viral replication in the CHI model.

To characterize the viral kinetics in the inoculation study (i.e., sentinel cohorts), blood sampling is recommended two times within day 1 after HCV challenge and then at days 3 and 7 postinfection for the pre-viremia phase[7,33]. Subsequently the measurements of HCV RNA levels could be measured twice weekly for 4 weeks and then weekly until spontaneous clearance or treatment initiation[7]. Although the inoculation study mentioned above would provide further information on the frequency of blood sampling as more data are accumulated, our modeling results show that a transient reduction between two phases of viral increase occurred within the first week post-infection (4.6 ± 0.4 days), which suggests that more frequent sampling especially around this time (~day 5 postinfection) probably is required to provide a more precise estimation regarding the early HCV RNA kinetics.

Our study has several limitations. First, HCV RNA levels were only measured in the serum of mice, and thus more experimental studies would be needed to investigate the effect of innate immune response, such as measuring the intrahepatic levels of interferon response genes such as 2OAS-1 mRNA expression as was previously done in the chimpanzee model[28]. Second, the data for the number of HCV-infected cells is not available because liver biopsies cannot be obtained during mouse infections without sacrificing the mice. If the number of infected cells could be measured at the initial stage of infection such as 6 h post infection, the fitting process of both ODE and ABM can be improved and therefore add another layer of model confidence. Third, we assumed in both ODE and ABM models no death of human hepatocytes nor proliferation based on previous reported stable hAlb levels during infection[21]. However, while the levels of hAlb indicate the overall extent of the mass of the human portion of the liver chimera and persistence of human hepatocytes, the presence of cytolytic clearance of human hepatocytes (and hepatocyte proliferation) cannot be excluded without other measured markers such as alanine transaminase (ALT). Lastly, the ODE model suggested two distinct virus populations with different infectivity rates, whereas the ABM model proposed a single virus population that releases virions after the eclipse phase, followed by subsequent virion production cycles. The ABM estimated an eclipse phase duration of 1–52 h, consistent with in vitro experiments[22], suggesting that ABM may be a more biologically-relevant model, as the two-virus population observed in ODE (without an eclipse phase) could be an artifact of the mean-field ODE modeling approach. Further experiments are necessary to verify the viral-host predictions suggested by ODE and ABM.

In conclusion, our study demonstrates the power and utility of using modeling approaches to gain comprehensive insights into the complexities of HCV-host interactions and supports the use of the liver-humanized mouse model for the CHI model development. Detailed viral kinetic data from CHI studies will provide the basis to extend and refine the mathematical models to dissect the impact of the innate and adaptative immune responses on early HCV infection in humans and to provide a guide to vaccine development and assessment.

Data availability

We provide all the raw data in Supplementary Table S3.

Received: 23 May 2024; Accepted: 11 December 2024
Published online: 30 December 2024

References

1. Martinello, M. et al. Hepatitis C. *Lancet* **402**, 1085–1096 (2023).
2. Osburn, W. O. et al. Spontaneous control of primary hepatitis C virus infection and immunity against persistent reinfection. *Gastroenterology* **138**, 315–324 (2010).
3. Dahari, H., Feinstone, S. M. & Major, M. E. Meta-analysis of hepatitis C virus vaccine efficacy in chimpanzees indicates an importance for structural proteins. *Gastroenterology* **139**, 965–974 (2010).
4. Wester, C. Hepatitis C virus clearance cascade—United, S. 2013–2022. *Morbidity and Mortality Weekly Report* 72 (2023).
5. Page, K. et al. Randomized trial of a vaccine regimen to prevent chronic HCV infection. *N. Engl. J. Med.* **384**, 541–549 (2021).
6. Liang, T. J. et al. Controlled human infection model-fast track to HCV vaccine? *N. Engl. J. Med.* **385**, 1235–1240 (2021).
7. Feld, J. J. et al. Controlled human infection model for hepatitis C virus vaccine development: trial design considerations. *Clin. Infect. Dis.* **77**, S262–S269 (2023).
8. Shteyer, E. et al. Modeling suggests that microliter volumes of contaminated blood caused an outbreak of hepatitis C during computerized tomography. *Plos one*. **14**, e0210173 (2019).
9. Dahari, H. et al. Mathematical modeling of primary hepatitis C infection: noncytolytic clearance and early blockage of virion production. *Gastroenterology* **128**, 1056–1066 (2005).
10. Collins, F. S. *NIH Will No Longer Support Biomedical Research on Chimpanzees* (National Institutes of Health, 2015).
11. DebRoy, S. et al. Hepatitis C virus dynamics and cellular gene expression in uPA-SCID chimeric mice with humanized livers during intravenous silibinin monotherapy. *J. Viral Hepat.* **23**, 708–717 (2016).
12. Shi, N. et al. Combination therapies with NS5A, NS3 and NS5B inhibitors on different genotypes of hepatitis C virus in human hepatocyte chimeric mice. *Gut* **62**, 1055–1061 (2013).
13. Osawa, M. et al. Efficacy of glecaprevir and pibrentasvir treatment for genotype 1b hepatitis C virus drug resistance-associated variants in humanized mice. *J. Gen. Virol.* **100**, 1123–1131 (2019).
14. Liang, T. J. et al. Challenge inoculum for hepatitis C virus controlled human infection model. *Clin. Infect. Dis.* **77**, S257–S261 (2023).
15. Hailegiorgis, A. et al. Modeling suggests that virion production cycles within individual cells is key to understanding acute hepatitis B virus infection kinetics. *PLoS Comput. Biol.* **19**, e1011309 (2023).
16. Ishida, Y. et al. Acute hepatitis B virus infection in humanized chimeric mice has multiphasic viral kinetics. *Hepatology* **68**, 473–484 (2018).
17. Tateno, C. et al. Generation of novel chimeric mice with humanized livers by using hemizygous cDNA-uPA/SCID mice. *PloS one*. **10**, e0142145 (2015).
18. Umehara, T. et al. Serine palmitoyltransferase inhibitor suppresses HCV replication in a mouse model. *Biochem. Biophys. Res. Commun.* **346**, 67–73 (2006).
19. Ahmadi-Noorbakhsh, S. et al. Anesthesia and analgesia for common research models of adult mice. *Lab. Anim. Res.* **38**, 40 (2022).
20. Reinharz, V. et al. Understanding hepatitis B virus dynamics and the antiviral effect of interferon alpha treatment in humanized chimeric mice. *J. Virol.* **95**, e0049220 (2021).
21. Matsumura, T. et al. Amphipathic DNA polymers inhibit hepatitis C virus infection by blocking viral entry. *Gastroenterology* **137**, 673–681 (2009).
22. Lindenbach, B. D. et al. Complete replication of hepatitis C virus in cell culture. *Science* **309**, 623–626 (2005).
23. Fortin, F-A. et al. DEAP: Evolutionary algorithms made easy. *J. Mach. Learn. Res.* **13**, 2171–2175 (2012).
24. Bäck, T., Fogel, D. & Michalewicz, Z. *Evolutionary Computation* (Institute of Physics Publishing, 2000).
25. Ozik, J. et al. From desktop to large-scale model exploration with Swift/T, in *WSC* (IEEE, 2016).
26. Zhong, J. et al. Persistent hepatitis C virus infection in vitro: coevolution of virus and host. *J. Virol.* **80**, 11082–11093 (2006).
27. Shekhtman, L. et al. Modeling hepatitis C virus kinetics during liver transplantation reveals the role of the liver in virus clearance. *Elife* **10**, e65297 (2021).
28. Major, M. E. et al. Hepatitis C virus kinetics and host responses associated with disease and outcome of infection in chimpanzees. *Hepatology* **39**, 1709–1720 (2004).
29. Major, M. E. et al. Previously infected and recovered chimpanzees exhibit rapid responses that control hepatitis C virus replication upon rechallenge. *J. Virol.* **76**, 6586–6595 (2002).
30. Feld, J. J. et al. Short-course, direct-acting antivirals and ezetimibe to prevent HCV infection in recipients of organs from HCV-infected donors: a phase 3, single-centre, open-label study. *Lancet Gastroenterol. Hepatol.* **5**, 649–657 (2020).
31. Kolykhalov, A. A. et al. Transmission of hepatitis C by intrahepatic inoculation with transcribed RNA. *Science* **277**, 570–574 (1997).
32. Barnes, E. et al. Implementation of a controlled human infection model for evaluation of HCV vaccine candidates. *Hepatology* **77**, 1757–1772 (2023).
33. Shoukry, N. H., Cox, A. L. & Walker, C. M. Immunological monitoring in hepatitis C virus controlled human infection model. *Clin. Infect. Dis.* **77**, S270–S275 (2023).

Acknowledgements

This work was supported, in part, by U.S. NIH grants R01GM121600, R01AI078881 and R01AI158666, Japan AMED grant JP23fk0310513 and Canadian Institutes of Health Research under AFF funding reference #178382. We gratefully acknowledge the computing resources provided on Bebop, a high-performance computing cluster operated by the Laboratory Computing Resource Center at Argonne National Laboratory. The funder of the study had no role in study design, data analysis, interpretation of the results, writing the report, or in the decision to submit the paper for publication.

Author contributions

Concept and design: KC, HD; Experimental (in vivo) data: YI, HAC, CTM, KC; In silico modeling: ZS, AM, AJ, HD; High-performance computing: NTC and JO; Writing of manuscript: ZS, AM, YI, AJ, JO, SJC, MM, HD; Supervision: JO, KC, HD; Funding acquisition: JF, KC, HD. All authors reviewed and approved the final version of the manuscript:

Declarations

Competing interests

YI and CTM are PhoenixBio employees. KC has received honoraria from Bristol-Myers Squibb and MSD K.K., AbbVie, Gilead Science, Dainippon Sumitomo Pharma and Mitsubishi Tanabe Pharma and research funding from Gilead Science, Dainippon Sumitomo Pharma, MSD K.K., AbbVie, Eisai, TORAY, Otsuka Pharma, Chugai Pharma, Takeda Pharma and Roche. JJF reports research funding and consulting fees from AbbVie and Gilead. All other authors have nothing to disclose.

Additional information

Supplementary Information The online version contains supplementary material available at https://doi.org/10.1038/s41598-024-83104-0.

Correspondence and requests for materials should be addressed to K.C. or H.D.

Reprints and permissions information is available at www.nature.com/reprints.

Publisher's note Springer Nature remains neutral with regard to jurisdictional claims in published maps and institutional affiliations.